Heteroatom Chemistry
Volume 00, Number 0, 2009

Tetrakis-Phthalocyanines Bearing Electron-Withdrawing Fluoro Functionality: Synthesis, Spectroscopy, and Electrochemistry

Ahmet T. Bilgiçli,[1] Mehmet Kandaz,[1] Ali Rıza Özkaya,[2] and Bekir Salih[3]

[1]*Department of Chemistry, Sakarya University, 54140 Esentepe, Sakarya, Turkey*

[2]*Department of Chemistry, Marmara University, 34722 Göztepe, Istanbul, Turkey*

[3]*Department of Chemistry, Faculty of Science, Hacettepe University, 06532 Beytepe Campus, Ankara, Turkey*

Received 23 December 2008; revised 12 April 2009

ABSTRACT: *In this study, 2,9,16,23-tetrakis-4′-(2,3,5,6-tetrafluoro)-phenoxy-phthalocyaninato-metalfree and metal(II) complexes, (H_2PcBzF_{16}, $ZnPcOBzF_{16}$, $CuPcOBzF_{16}$, and $CoPcOBzF_{16}$) (Bz: Benzene) (2H, Zn, Cu, and Co), have been prepared directly from the corresponding 4′-(2,3,5,6-fluorophenylthio)-phthalonitrile compounds in the presence of 1,8-diazabicyclo[5.4.0]undec-7-ene (DBU) in high boiling quinoline solvent. Tetrafluoro atoms on 2,3,5,6-position of benzene at the peripheral sites of phthalocyanines (Pcs) give rise interesting solubility to tetrakismetallophthalocyanines. Although all complexes were soluble in DCM, $CHCl_3$, THF, DMF, and DMSO with increasing order, complexes synthesized, particularly H_2PcBzF_{16}, $CuPcOBzF_{16}$, have very limited solubility in DMF and DMSO. The complexes have been characterized by elemental analysis, FTIR, ^1H NMR, UV–vis, and MALDI–TOF mass spectral data. The cyclic voltammetry and differential pulsed voltammetry of the complexes show that while H_2PcBzF_{16}, $CuPcOBzF_{16}$, and $ZnPcOBzF_{16}$ give ligand-based reduction and oxidation processes, $CoPcOBzF_{16}$ gives both ligand and metal-based redox processes, in harmony with the common metallophthalocyanine complexes. Redox processes due to both aggregated and disaggregated species were simultaneously observed during the first reduction process. The nature of the metal-based redox processes was confirmed using spectroelectrochemical measurements.* © 2009 Wiley Periodicals, Inc. Heteroatom Chem 00:1–10, 2009; Published online in Wiley InterScience (www.interscience.wiley.com). DOI 10.1002/hc.20545

INTRODUCTION

Phthalocyanines have varied chemistry resulting from their rich π-electron system, and thus are known as excellent modifiable functional materials [1–3]. Accordingly, there are literally hundred of publications and patents related to their various technological fields [4–6]. Because of their very high tinctorial nature, diverse redox chemistry, and high thermal and chemical stability, various applications such as semiconductivity [7], electrochromic displays [8], chemical sensors [9], and optical properties [10,11] have prompted the researchers to synthesize various types of metallophthalocyanines (MPcs) recently [3–8,12–14]. Introducing electron donor

Correspondence to: Mehmet Kandaz; e-mail: mkandaz@sakarya.edu.tr.
Contract grant sponsor: Research Fund of Sakarya University.
Contract grant sponsor: TBAG.
Contract grant number: 108T094.

and acceptor groups into the phthalocyanine (Pc) ring strongly affects its spectral, electrical, and electrochemical properties. Tetra- and octa-substituted MPcs have higher chemical stability as compared to unsubstituted ones. Electron-withdrawing substituents at the periphery of the macrocycle cause a large increase in the ionization potential of the system, protect the MPc from oxidative destruction [15–17], and thus enhance its catalytic activity. From the viewpoint of organic semiconductors, it is known that substitution of electron donor and acceptor groups leads to *p*-type and *n*-type characteristics of the Pc ring, respectively [7,18–20].

The main problem limiting applications of phthalocyanines (Pcs) in many fields is still their limited solubility. Their solubility can be increased, however, by introducing electron-withdrawing (—F, —Cl, —Br) and electron-donating (—NH_2, Ar—S—, RO—, RS—) bulky or long chain alkyl groups into the peripheral sites [21–25]. The formation of constitutional isomers and the higher dipole moment of the tetrasubstituted Pcs resulting from the unsymmetrical arrangement of the substituents on the periphery leads to higher solubility of Pcs in many organic solvents [26].

Redox processes of Pcs can be shifted by electron-withdrawing and/or electron-repelling groups [22]. Thus, fluorinated MPcs are currently receiving a great deal of attention due to electron-withdrawing nature of fluorine atoms [17,27]. Although many studies on the chemistry of MPcs in solution, which have been limited to Pc with electron-donating substituents, have been carried out, those with electron-attracting groups, especially containing fluorine atoms, have not been extensively studied [17,22,27,28].

Here, we report the synthesis and characterization of a new ligand, 4′-(2,3,5,6-fluorophenylthio)-phthalonitrile, obtained through 2,3,5,6-fluorolthiophenol and 4-nitrophthalonitrile in the presence of K_2CO_3 in dimethylformamide (DMF) and its complexes. We also investigate their redox properties by cyclic and differential pulse voltammetry and spectroelectrochemistry.

RESULTS AND DISCUSSION

Synthesis and Characterization

Fluoro functional MPcs **3–5** were prepared by the templated cyclization from 4′-(2,3,5,6-tetrafluorophenylthio)-phthalonitrile, **1**, and anhydrous metal salts, $Zn(OAc)_2$, $CuCl_2$, and $CoCl_2$ in quinoline in the presence of 1,8-diazabicyclo[5.4.0]undec-7-ene (DBU) as a strong base at 170–185°C. Metal-free Pc **2** was obtained in *N*,*N*-dimethylamino ethanol under N_2 atmosphere, also in the presence of DBU as a strong base (Scheme 1). The blue cyclotetramerization products **2–5** were purified by column chromatography in moderate yield (40% for **2**, 44% for **3**, 32% for **4**, and 37% for **5**). Elemental analysis results and the spectral data (^{1}H NMR, FTIR, and MALDI–TOF MS) of all the new products are consisted with the assigned formulations. The phthalocyanine products (M = 2H, Zn, Cu, and Co) were isolated as a mixture of isomers as expected. The presence of isomers could be verified with slight broadening encountered in the UV–vis absorption bands and broadening in the ^{1}H NMR when compared with those of octa-substituted Pcs composed of a single isomer [13,15, 26a]. All the analytical and spectral data are consistent with the predicted structures. The 16 peripheral fluoro atoms confer on these molecules moderate solubility in halogenated solvents and good solubility in THF, DMF, DMSO, and DMAA, in comparison with unsubstituted Pcs.

The FTIR spectra of Pcs involved strong —*C*—*F* stretching band on the periphery with small shifts in comparison with that of **1**. In the meantime, —*CN* band at 2226 cm^{-1} in the spectrum of **1** disappeared after Pc formation. Aliphatic —*C*—*H* and aromatic =*C*—*H* peaks at above and below 3000 cm^{-1} and the rest of the spectra were closely similar to those of compound **1**, and diagnosed easily.

The ^{1}H NMR spectra of **2** and **3** were almost identical with starting compound **1** except small shifts and core NH signal in **2**. The —*NH* protons in the inner core of the **2** were also very well characterized by the ^{1}H NMR spectroscopy, which showed a peak at −1.52 ppm as a result of the 18 π-electron system of the Pc ring [22]. The aromatic protons in the lower field region and 12 different aromatic carbon atoms between 110 and 160 ppm in the ^{1}H NMR spectrum are the most distinctive signals for the characterization of **1**. The rather broad bands in the case of **2** and **3** were probably due to both chemical exchange associated with aggregation–disaggregation equilibria that occur at high concentrations used in the NMR measurements and the fact that the products obtained in these reactions are the mixture of four positional isomers, which are expected to show chemical shifts only slightly differing from each other [1,26a].

UV–vis spectra of the Pc complexes exhibit characteristic Q and B bands in DMSO. Two principle π–π^* transitions are seen for Pcs: a lower energy Q band (~650–750 nm, π–π^* transition from the highest occupied molecular orbital (HOMO) to the lowest unoccupied molecular orbital (LUMO) of

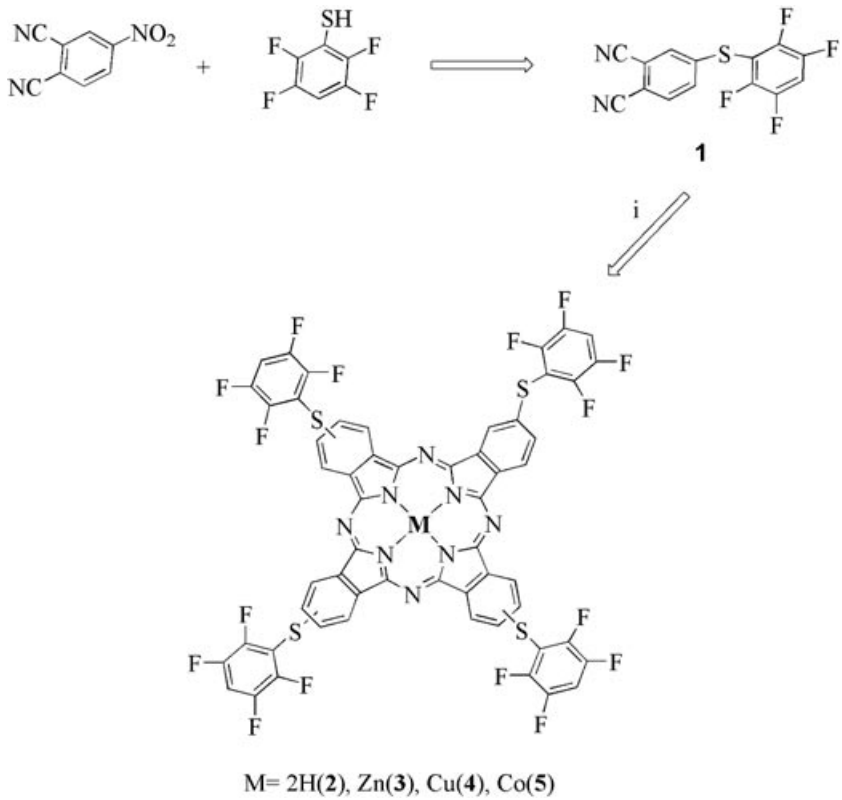

SCHEME 1 Synthetic route of 4′-(2,3,5,6-Tetrafluorophenylthio)phthalonitrile (1) and its free and metal complexes (M = 2H, Zn(II), Cu(II), Co(II). (i) 2,3,5,6-Tetrafluorothiophenol and 4-nitrophthalonitrile and K_2CO_3 in DMF at 40°C for 24 h. (ii) anhydrous Zn $(acac)_2$, $CuCl_2$, and $CoCl_2$, DBU , quinoline.

the complexes) and a higher energy B band {∼300–350 nm, deeper π–π^* transition from the highest occupied MOs (a_{1u} and a_{2u}) to the LUMO (e_g)} [2]. The Q-band absorptions in the UV–vis absorption spectra of all MPcs were observed as a single band of high intensity due to a single π–π^* transition with shoulders at slightly higher energy side of the Q band (681 nm for **3**, 678 nm for **4**, and 672 nm for **5)** as seen in Fig. 1. The small differences between the absorption bands of synthesized compounds are due to the ionic radius of the metal centers. The metal-free Pc **2** showed splitting of Q band as expected (Q_x = 671 nm and Q_y = 703 nm) with a shoulder at the higher energy side of the Q band. The effect of *S*-substitution on the periphery for all Pcs when compared with those of *O*-substituted derivatives was the shift of Q bands to longer wavelengths [3,8,13–15,21–27]. On the other hand, the Q band position of the Pcs bearing electron-withdrawing fluoro functional groups shifted to shorter wavelengths, compared with nonfluorinated thio- or phenoxy-substituted compounds, as expected [17,27].

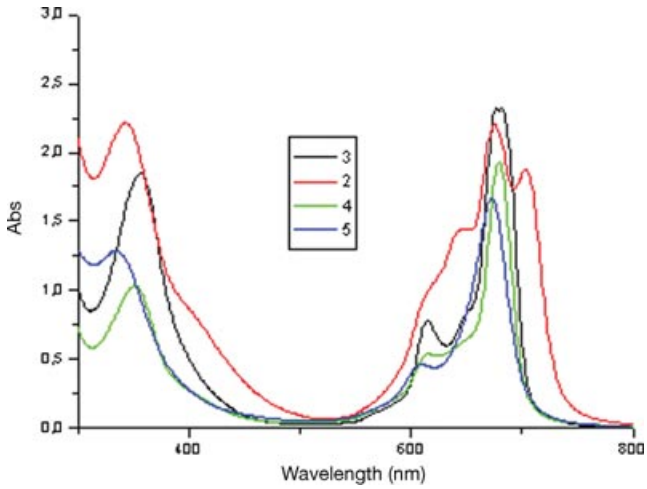

FIGURE 1 UV–visible spectra of **2–5** in DMSO.

MALDI–TOF Mass Spectra

Positive ion and reflectron mode MALDI–TOF mass spectrum of **2** was carried out using α-cyano-4-hydroxycinnamic acid MALDI matrix (Fig. 2). Protonated molecular ion peak was observed at 1234.20 Da with the other isotopic peaks mainly resulting

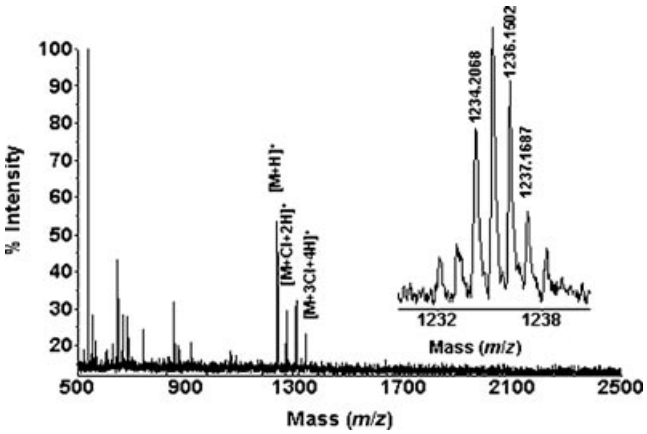

FIGURE 2 Positive ion and reflectron mode MALDI–TOF mass spectrum of **2** was obtained in α-cyano-4-hydroxycinnamic acid MALDI matrix using N_2 laser accumulating 50 laser shots. Inset spectrum shows expanded molecular mass region of the complex.

from the isotopic distribution of carbon, which overlaps with the mass of **2** calculated theoretically from its elemental composition.

Figure 3 shows the MALDI–TOF mass spectra of **3**. For **3** and **4**, all high-resolution MALDI–TOF mass spectra were obtained most efficiently using only dithranol MALDI matrix compared to the other novel MALDI matrices. Mainly protonated molecular ion peaks and the dithranol peak at around 227 Da were characterized for **3** and **4**. It was concluded that all experimental isotopic peak distributions of protonated molecular ions overlapped completely with their theoretical calculated isotopic peak distributions. All MALDI–TOF results showed that

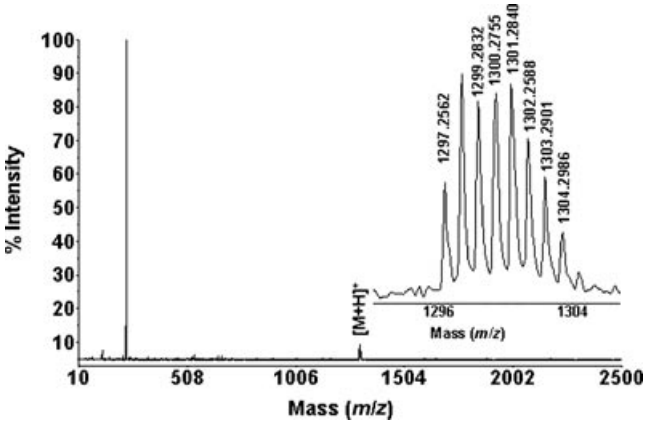

FIGURE 3 Positive ion and reflectron mode MALDI–TOF mass spectrum of **3** was obtained in dithranol (1,8-dihydroxy-10*H*-anthracen-9-one) MALDI matrix using nitrogen laser accumulating 50 laser shots. Inset spectrum shows expanded molecular mass region of the complex.

Dithranol was a suitable matrix for these types of metal complexes to get clearer MALDI–TOF mass spectrum, and also it could be concluded that metal complexes of these ligands were more stable in dithranol matrix. Positive ion and reflectron mode MALDI–TOF mass spectrum of **5** was obtained as high-resolution spectrum without any fragmentation in dithranol matrix. Experimental isotopic peak distributions of protonated molecular ion peak of this complex overlapped exactly with its theoretical calculated isotopic peak distributions. This information gives the full characterization of this complex by MALDI–TOF mass spectroscopy [26a,26b]. The results showed that the complexes were characterized precisely by MALDI–TOF mass spectroscopy.

Electrochemical Measurements

Cyclic and differential pulse voltammetry of **2**–**5** were carried out on a platinum working electrode in DMSO. Controlled-potential coulometry studies showed that the redox processes monitored for these compounds generally involve the transfer of one electron. Voltammetric data of the compounds are presented in Table 1.

Compound **2** displayed three reduction waves at $E_{1/2} = -0.54$ V, $E_{1/2} = -0.81$ V, and $E_{1/2} = -1.57$ V versus saturated calomel electrode (SCE), with characteristic anodic to cathodic peak separations for one-electron transfer processes (Fig. 4A). These Pc ring-based redox processes were examined as a function of potential scan rate to determine the mode of mass transport. The anodic-to-cathodic peak current ratio for the first reduction couple (II) is higher than unity. In addition, this ratio increases noticeably with increasing scan rate while the cathodic peak becomes sharp. These observations suggest that compound **2** is adsorbed on the electrode surface. When the electrode is left in solution for a long time before the first scan, the effect of adsorption on the peak current ratio was more pronounced. On the other hand, in the case that the voltammetric cycle was continued at a constant scan rate, the anodic-to-cathodic peak current ratio for couple II decreased with the scan number, suggesting that the adsorbed species are lost from the surface during the first reduction process. The cathodic peak currents of the couples II–IV increased in direct proportion to the square root of the scan rate between 0.025 and 0.500 V s^{-1}, thus suggesting that the relevant reactions are controlled by diffusion. The first oxidation process of metal-free Pcs could not be detected usually in the studies reported previously [29–31]. Differential pulse voltammetry enabled us to identify the first oxidation process of **2** at 0.96 V versus SCE without the

TABLE 1 Voltammetric Data for **2, 3, 4**, and **5**

Compound	*Redox Couple*	$E_{1/2}$ *(V)*[a] *versus SCE and Fc/Fc*$^{+}$[b]	ΔE_p *(V)*[c]
2	Pc(–1)/Pc(–2) (I)	0.96 (0.46)[d]	–
	Pc(–2)/Pc(–3) (II)	−0.54 (−1.04)	0.080
	Pc(–3)/Pc(–4) (III)	−0.81 (−1.31)	0.060
	Pc(–4)/Pc(–5) (IV)	−1.57 (−2.07)	0.060
3	Pc(–1)/Pc(–2) (I)	0.67 (0.17)	0.080
	Pc(–2)/Pc(–3) (II)	−0.78 (−1.28)	0.060
	Pc(–3)/Pc(–4) (III)	−1.19 (−1.69)	0.060
	Pc(–4)/Pc(–5) (IV)	−1.46 (−1.96)	0.060
4	Pc(–1)/Pc(–2) (I)	0.61 (0.11)	0.070
	Pc(–2)/Pc(–3) (II)	−0.75 (−1.25)	0.100
	Pc(–3)/Pc(–4) (III)	−0.94 (−1.44)	0.080
	Pc(–4)/Pc(–5) (IV)	−1.63 (−2.13)	0.140
5	Co(III)/Co(II) (I)	0.49 (−0.01)	0.100
	Co(II)/Co(I) (II)	−0.41 (−0.91)	0.060
	Pc(–2)/Pc(–3) (III)	−1.15 (−1.65)	0.060
	Pc(–3)/Pc(–4) (IV)	−1.62 (−2.12)	0.200

[a] $E_{1/2} = (E_{pa} + E_{pc})/2$ at 0.050 V s^{-1}.
[b] The values in parenthesis indicate the potentials versus Fc/Fc^{+}.
[c] $\Delta E_p = E_{pa} - E_{pc}$ at 0.050 V s^{-1}.
[d] This value is the anodic peak potential, which could be identified only by differential pulse voltammetry.

corresponding cathodic peak (peak I in Fig. 4B). The difference between the first oxidation and the first reduction process is 1.50 V. This difference corresponds to the gap between the HOMO and the LUMO and is consistent with the previously reported values for metal-free Pcs [29,32].

Figure 5 indicates cyclic and differential pulse voltammograms of **4**. When the potential of the working electrode was scanned toward negative potentials starting at 0 V versus SCE, compound **4** displayed four reduction peaks whereas three corresponding reoxidation peaks were observed during the reverse scan. The first two reduction processes for MPcs are separated by about 0.30–0.40 V [1]. However, the difference between the first two reduction peaks (II′ and II) was about 0.10–0.20 V, depending on the scan rate. The current ratio of

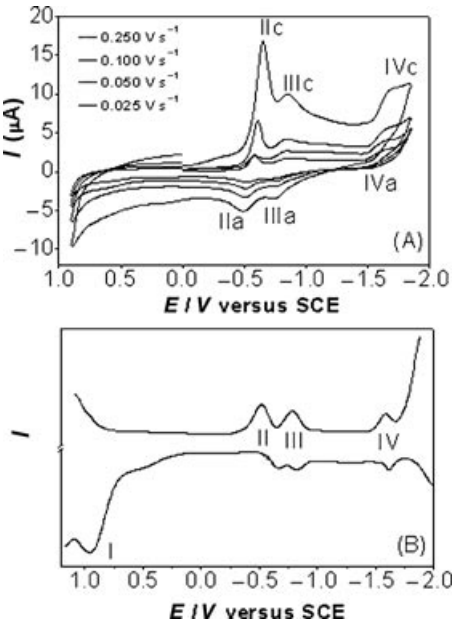

FIGURE 4 Cyclic (A) and differential pulse (B) voltammograms of **2** in DMSO–TBAP solution.

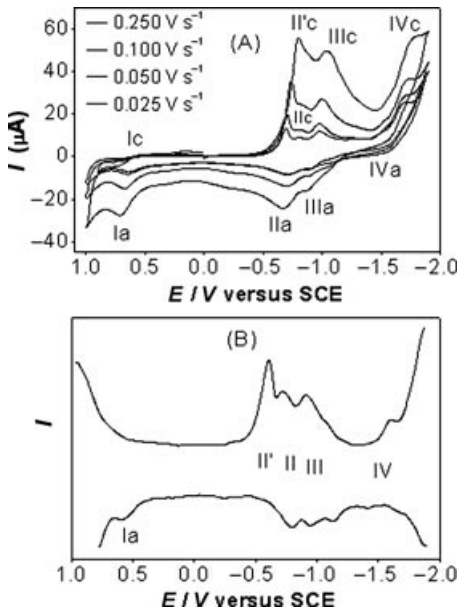

FIGURE 5 Cyclic (A) and differential pulse (B) voltammograms of **4** in DMSO–TBAP solution.

these peaks (II'_c/II_c) was observed to increase with increasing scan rate, and became finally a composite wave at high scan rates. Surprisingly, there was no any potential difference between the peaks IIa and II'_c at 0.050 while peak II'_c appeared unusually at less negative potentials with respect to peak IIa at the scan rates lower than 0.050 V s^{-1}. These observations also imply the adsorption of compound **3** on the electrode surface. Another possible and additional effect associated with the first two reduction processes is the presence of equilibrium between the aggregated and disaggregated species since couple II is split at low scan rates. It is possible that peaks II'_c and II_c correspond to the reduction of aggregated and disaggregated species, respectively. In the case that aggregation–disaggregation equilibrium is slow relative to the electrochemical time scale, reduction processes due to both species could simultaneously be monitored. Moreover, the current ratio of peak II'_c to peak II_c decreased with dilution (Fig. 6). This provided additional support for the presence of aggregated and disaggregated species. The similarities between the redox behavior of **2** and **4**, in general, both indicating three one-electron reduction couples and a one-electron oxidation process (Table 1), show that redox processes of **4** are also ligand based, and Cu(II) metal center is not redox active. The redox processes of **4** occur at the potentials more negative than those of **2**. This can be attributed to the difference in the polarizing power of the central metal and hydrogens [29]. As compared with **4**, similar redox behavior was observed with compound **3** with some differences in redox potentials, which can be attributed to the differences in polarizing power of different metal centers (Table 1). The redox potentials measured for **2–4** are consistent with the general redox characteristics reported previously for similar Pcs, being less

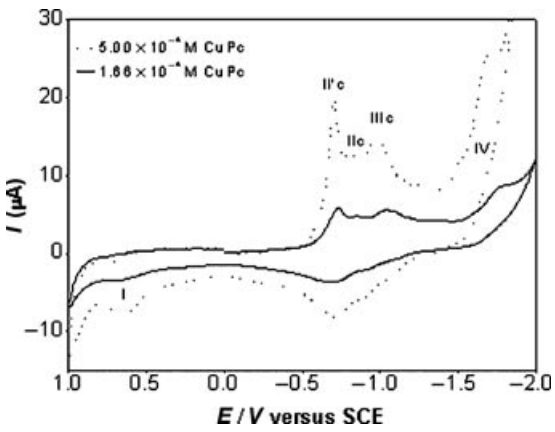

FIGURE 6 Cyclic voltammograms of **4** at two different concentrations at 0.100 V s^{-1} in DMSO–TBAP solution.

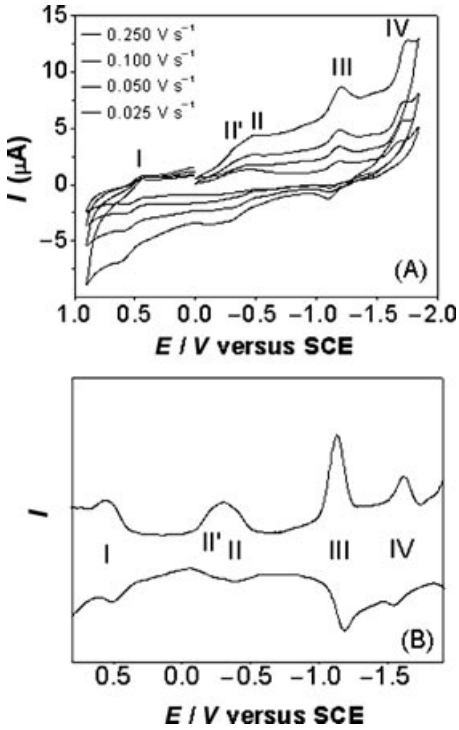

FIGURE 7 Cyclic (A) and differential pulse (B) voltammograms of **5** in DMSO–TBAP solution.

negative as compared with those given for unsubstituted Pcs in the literature [29]. This positive potential shift can be attributed to the electron-withdrawing effect of fluorine atoms in the complexes. Therefore, it was possible to observe the third reduction process for these complexes, which cannot be monitored generally.

Typical cyclic and differential pulse voltammograms for **5** are shown in Fig. 7. Although it also indicates three one-electron reduction processes at $E_{1/2} = -0.41$ V, $E_{1/2} = -1.15$ V, and $E_{1/2} = -1.62$ V versus SCE, and a one-electron oxidation process at $E_{1/2} = 0.49$ V versus SCE (Table 1), the redox potentials of **5** are different from those of other compounds. If the transition metal ion at the center has no accessible d orbital levels lying between the HOMO and LUMO gap of a Pc species, then its redox chemistry will appear very much like that of a main group Pc species. The nickel, copper, zinc, and some other MPcs behave in this fashion, with the M(II) central ion being unchanged as the MPc unit is either oxidized or reduced. On the other hand, MPcs, such as MnPc, CoPc, and FePc, having a metal that possesses energy levels lying between the HOMO and the LUMO of the Pc ligand, in general exhibit redox processes centered on the metal [29,30,33–36]. In addition, these species vary

their electrochemical behavior according to their environment, i.e., the oxidation of Co(II)Pc(–2) can lead to $[Co(III)Pc(-2)]^+$ or $[Co(II)Pc(-1)]^+$ depending on whether there are any available suitable coordinating species that would stabilize the Co(II) center. Such electrochemistry, especially of Co(II)Pc(–2) and Fe(II)Pc(–2), is split into two sections that referring to donor solvents and nondonor solvents. The main difference lies in whether metal or the ring is oxidized first. Donor solvents strongly favor Co(III)Pc(–2) by coordinating along the axis to form six coordinate species. If such donor solvents are absent, then oxidation to Co(III) is inhibited and ring oxidation occurs first. Thus, the first oxidation and the first reduction processes of **5** are probably metal based and correspond to Co(II)Pc(–2)/$[Co(III)Pc(-2)]^+$ and Co(II)Pc(–2)/$[Co(I)Pc(-2)]^-$, respectively, while the second and third reductions are ring based, since the voltammetric measurements were carried out in DMSO–TBAP. It was observed that the shape of the couple II (Fig. 7A), corresponding the first reduction process of **5**, is strongly affected by the scan rate. This is probably due to the aggregation–disaggregation equilibrium. It appears that at high scan rates at which aggregation–disaggregation equilibrium is slow with respect to the time scale of electrochemical measurement, the first reduction process is split into two waves (II′ and II), corresponding to the reduction of aggregated and disaggregated species. This behavior was well characterized by rounded shape of couple II in cyclic and differential pulse voltammograms (Fig. 7). However, adsorption on the electrode surface is not observed for **5**.

To provide additional support for the identification of the metal-based redox processes of **5**, spectroelectrochemistry of this complex was also studied. Typical absorption spectra for the original **5** and its electrochemically generated species are shown in Fig. 8. Figure 8A shows the UV–vis spectral changes of **5** during its first reduction at −0.60 V versus SCE. The Q band absorption at 672 nm shifts to 713 nm, while new band at 485 nm appears with a shoulder around 441 nm. The spectral changes have well-defined isosbestic points at 293, 399, 564, and 697 nm. The new band at 485 nm and shifting of the Q band indicate the formation of $[Co(I)Pc(-2)]^-$ species, confirming that first reduction of **5** occurs at the metal center [37]. Upon the second reduction at −1.30 V versus SCE, the Q band absorption at 713 nm and the shoulder at 441 nm decrease without shift (Fig. 8B). In the meantime, the absorption at 485 nm increases slightly in intensity with the redshift to 490 nm while the absorption between 500 and 600 nm increases. Clear isosbestic points

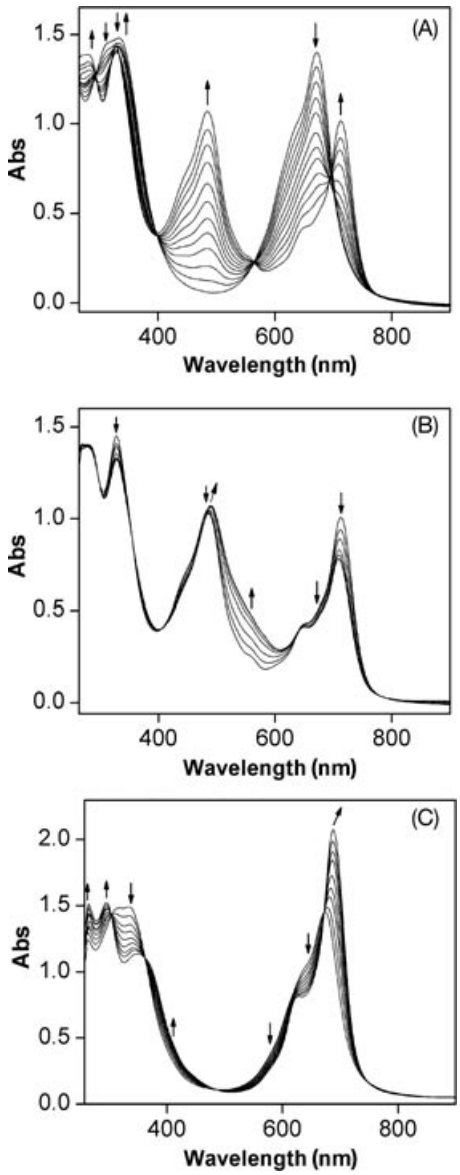

FIGURE 8 In situ UV–vis spectral changes during (A) the first reduction, (B) the second reduction, and (C) the first oxidation processes of **5**.

were observed at 355, 406, 640, and 784 nm. These spectral changes at the potential of the couple III are characteristic for a ring-based reduction in complex **5**, confirming our voltammetric assignment of this process to $[Co(I)Pc(-2)]^-/[Co(I)Pc(-3)]^{2-}$ [38]. Figure 8C shows the spectral changes during oxidation of **5**. The original Q band absorption at 672 nm increases with a clear shift to 687 nm. In the meantime, the absorption at the red side of the shoulder at around 616 nm decreases. These spectral changes, especially the shift in the Q band absorption, are typical of Co(II)Pc(–2)/$[Co(III)Pc(-2)]^+$ redox process

[38] and result in the isosbestic points at 303, 361, 485, and 672 nm, together with those in the B band region.

EXPERIMENTAL

2,3,5,6-Fluorolthiophenol, 4-nitrophthalonitrile diethyl ether, tetrahydrofuran (THF), tetrabutylammonium tetrafluoroborate, MX_2(M = Zn , Cu, and Co; X = O_2CMe and Cl) and 4-nitrophthalonitrile were purchased from Merck (Darmstadt, Germany) and Alfa Aesar (Karlsruhe, Germany) Chemical Co. and were used as received. THF was distilled from anhydrous $CaCl_2$ and acetophenon. Chromatography was performed with silica gel from Aldrich. All other reagents were obtained from Merck, Aldrich, and Alfa Aesar Chemical Co. and were used without purification. All reactions were carried out under dry N_2 atmosphere unless other was noted, and homogeneity of the products was tested in each step by TLC (silica gel, chloroform ($CHCl_3$), hexane, and methanol (MeOH)). FTIR spectra (KBr) were recorded on ATI UNICOM-Mattson 1000 spectrophotometer. Elemental analysis (C, H, and N) was performed at the Instrumental Analysis Laboratory of Marmara University. Routine UV–visible spectra were obtained in a quartz cuvette on a Unicom UV-2 spectrometer. ^{1}H NMR and ^{13}C NMR spectra were recorded on a Bruker 300 spectrometer. Multiplicities are given as s (singlet), d (doublet), and t (triplet). Mass spectra were acquired on a Voyager-DE™ PRO MALDI–TOF mass spectrometer (Applied Biosystems, USA) equipped with a nitrogen UV–laser operating at 337 nm, both in linear and reflectron modes with average of 50 and 100 shots for linear and reflectron modes.

MALDI samples were prepared by mixing sample solutions (4 mg/mL) with the matrix solution (1:10 v/v) in a 0.5-mL Eppendorf® micro tube. Finally, 1 μL of this mixture was deposited on the sample plate, dried at room temperature, and then analyzed. α-Cyano-4-hydroxycinnamic acid (15 mg/mL 1:1 water–acetonitrile) MALDI matrix for **2** and Dithranol (1,8-dihydroxy-10*H*-anthracen-9-one) (20 mg/mL THF) MALDI matrix for **3–5** were prepared. MALDI samples were prepared by mixing complex (2 mg/mL in acetonitrile) with the matrix solution (1:10 v/v) in a 0.5-mL Eppendorf® micro tube. Finally, 1 μL of this mixture was deposited on the sample plate, dried at room temperature, and then analyzed [8,22,26a]. The cyclic voltammetry and controlled potential coulometry (CPC) measurements were carried out with a Princeton Applied Research model VersoStat II potentiostat/galvanostat controlled by an external PC and utilizing a three-electrode configuration at 25°C. The working electrode was a platinum plate with a surface area of 0.10 cm^2. The surface of the working electrode was polished with a H_2O suspension of Al_2O_3 before each run. The last polishing was done with a particle size of 50 nm. A platinum wire served as the counterelectrode. Saturated calomel electrode was employed as the reference electrode and separated from the bulk of the solution by a double bridge. The ferrocene/ferrocenium couple (Fc/Fc^+) was also used as an internal standard. Electrochemical-grade tetrabutylammonium perchlorate (TBAP) in extra pure dimethylsulfoxide (DMSO) was employed as the supporting electrolyte at a concentration of 0.10 mol dm^{-3}. High purity N_2 was used for deoxygenating the solution at least 20 min prior to each run and to maintain a nitrogen blanket during the measurements. For CPC studies, Pt gauze working electrode (10.5 cm^2 surface area), platinum wire counterelectrode, separated by a glass bridge, and SCE as a reference electrode were used. The spectroelectrochemical measurements were carried out on an Agilent model 8453 diode array spectrophotometer equipped with the potentiostat/galvanostat and utilizing a three-electrode configuration of thin layer quartz spectroelectrochemical cell at 25°C. The working electrode was transparent platinum gauze. Platinum wire counterelectrode separated by a glass bridge and a SCE reference electrode separated from the bulk of the solution by a double bridge were used.

4′-(2 3,5,6-Tetrafluorophenylthio)-phthalonitrile **1**

2,3,5,6-Tetrafluorothiophenol (1.05 g, 6.35 mmol, excess) and 4-nitrophthalonitrile (1.00 g, 5.78 mmol) were dissolved in dry DMF (10 cm^3) and heated at 40°C in N_2 atmosphere for 1 h. Then finely ground anhydrous potassium carbonate (∼1.0 g excess) was added portionwise to mixture over the period of 0.5 h at 30°C. After the reaction mixture was kept at this temperature under N_2 atmosphere for 2 days, it was cooled to room temperature and poured in to c.a. 200 mL ice water. The creamy precipitate formed was filtered and dissolved in $CHCl_3$ and washed with 5% $NaHCO_3$ to remove starting uncreated compounds. The creamy solution was then dried with anhydrous Na_2SO_4 and filtered. It was chromatographed over a silica gel column using a mixture of $CHCl_3$:MeOH (100/5) as eluent, giving blue powder **1**. Finally, the pure powder was dried in a vacuum. Yield: 1.32 g (66%); mp = 156°C; Anal. Calcd for $C_{14}H_4F_4N_2S$ (308 g/mol): C, 54.55; H, 1.30; N, 9.09. Found: C, 54.20; H, 1.32; N, 8.83. IR (thin film) ν: (cm^{-1}); 3100 (w,

Ar—H), 3051 (w, Ar—CH), 2226 (C≡N, st), 1627, 1604 (C=C), 1577 (C=N), 1492 (st), 1438, 1377 (—C—F), 1272 (Ar—S—Ar), 1234, 1188, 1072, 914 (st) 891, 871, 837, 709, 524. ^{1}H NMR (DMSO-d_6) δ: 8.30 (s, H, ortho to Ar—C—S), 8.10 (dd, H, ortho to CN) , 8.02 (dd, H, meta to CN), 6.82 (ortho to Ar—C—F); ^{13}C NMR ([D_6]-DMSO) δ: 148.8 (Ar—C—F), 148.8 (Ar—C—F), 147.3 (Ar—C—F), 147.3 (Ar—C—F), 140.7 (Ar—C—S), 136.2 (Ar—C, ortho to Ar—C—S), 135.1 (Ar—C— ortho to Ar—C—CN), 131.5 (Ar—C , ortho to Ar—C—CN), 117.4 (Ar—C— ortho to CN), 116.54 (Ar—CN), 116.52 (Ar—CN), 114.3 (Ar—C— ortho to CN), 109.0 (Ar—C, ortho to Ar—S), 106.4 (Ar—C, ortho to Ar—C—F). EI/MS *m/z*: 308.2 [M$^+$].

2,9,16,23-Tetrakis-4′-(2,3,5,6-tetrafluorophenylthio)-phthalocyaninatometal-free **2**

A mixture of **1** (0.10 g; 0.32 mmol), DBU (0.05 mL), and dry *N*-*N*-dimethylaminoethanol was heated with stirring to 150–160°C for 12 h under N_2 atmosphere in a sealed tube. The deep green-blue product was cooled to room temperature and a waxy solid was washed successively with MeOH several times to remove any inorganic and organic impurities, until the filtrate was clear. Further purification was carried out by column chromatography with silica gel (eluent: $CHCl_3$/MeOH; 10/1, and then THF) and dried in vacuum. Compound **1** is less soluble than metal-substituted ones in both halogenated and polar solvent mentioned above.

Yield: 0.25 g (40%); mp >200°C; Anal. Calcd for $C_{56}H_{16}F_{16}N_8S_4$ (1232 g/mol): C, 54.55; H, 1.30; N, 9.09. Found: C, 53.88; H, 1.26; N, 8.92%. FTIR (KBr) ν (cm^{-1}): 3290 (NH), 3053 cm^{-1} (w, Ar—H, broad), 1627 (w), 1603 (C=C), 1490 (st), 1431, 1377, 1309 (st, —C—F), 1234 (Ar—S—Ar), 1176, 1109, 1068, 916 (st), 889, 848, 740, 711.; ^{1}H NMR (DMSO-d_6) δ: 8.32 (s, br, H, ortho to Ar—C—S), 8.12 (dd, br, H, ortho to CN) , 7.94 (dd, br, H, meta to CN), 6.72 (ortho to Ar—C—F), −1.54 (2H, br, core NH); UV–vis (DMSO), λ_{max} (nm): 703 (Q_x), 671 (Q_y), 644 (agg), 614, 342(B). MS (MALDI–TOF, CHCA as matrix) *m/z*: 1233 [M + H]$^+$.

2,9,16,23-Tetrakis-4′-(2,3,5,6-tetrafluorophenylthio)-phthalocyaninatozinc(II) **3**

A mixture of compound **1** (0.10 g; 0.32 mmol) anhydrous Zn $(O_2CMe)_2$ (0.015 g; 0.082 mmol), dry quinoline (2 mL), and DBU (0.05 mL) to a sealed tube was heated with efficient stirring at 170–180°C for about 8 h under N_2 atmosphere. After cooling to room temperature, resulting powder solid was washed several times successively with hexane, MeOH, and filtered to remove any inorganic and organic impurities until the filtrate was clear. The blue product was isolated by silica gel column chromatography with $CHCl_3$ to remove unreacted starting impurities and then with THF/$CHCl_3$ (1:2 v/v) as eluent to obtain main crude product and then dried in vacuo. This product is soluble in $CHCl_3$, acetone, THF, DMF, DMSO, and pyridine. Yield: 0.28 g (44%); mp >200°C; Anal. Calcd For $C_{56}H_{16}F_{16}N_8S_4Zn$ (1297 g/mol): C, 51.81; H, 1.23; N, 8.64. Found: C, 51.77; H, 1.26; N, 8.54%. FTIR (KBr) ν (cm^{-1}): 3066 (w, broad, Ar—H), 1722 (vw), 1627 (C=C), 1487 (st C—F), 1435 (w), 1381, 1306, 1232 (*Ar—S—Ar*), 1180, 1097, 1037, 916 (st), 889, 740 (Ar—F, bending), 707. ^{1}H NMR (DMSO-d_6) δ: 8.22 (s, H, ortho to Ar—C—S), 8.07 (dd, H, ortho to CN) , 8.90 (dd, H, meta to CN), 6.77 (ortho to Ar—C—F); UV–vis (DMSO), λ_{max} (nm): 681 (Q), 644 (agg), 613, 357 (B); MS (MALDI–TOF, Ditranol as matrix) *m/z* : 1297.26 [M + H]$^+$.

2,9,16,23-Tetrakis-4′-(2,3,5,6-tetrafluorophenylthio)-phthalocyaninatocopper(II) **4**

A mixture of compound **1** (0.10 g; 0.32 mmol), anhydrous $CuCl_2$ (0.01 g; 0.08 mmol; left one night in oven at 110°C), and DBU (0.05 mL) in dry quinoline was heated to 180°C under N_2 atmosphere for 8 h (1.00 mL). After cooling to room temperature and diluting with MeOH several times to remove any inorganic and organic impurities, it was filtered. The dark-blue crude product was treated several times with MeCN and filtered off. It was then successively washed with MeOH, diethyl ether and dried, and further purified by column chromatography with silica gel (eluent: $CHCl_3$:MeOH; 10:1, and then THF) and dried in vacuo. The desired compound is moderately soluble in $CHCl_3$ and soluble in acetone, THF, DMF, DMSO, and quinoline.

Yield: 0.196 g (32%); mp >200°C; Anal. Calcd for $C_{56}H_{16}F_{16}N_8S_4Cu$ (1295.5 g/mol): C, 51.88; H, 1.22; N, 8.64. Found: C, 51.13; H, 1.21; N, 8.01%. FTIR (KBr) ν (cm^{-1}): 3060 cm^{-1} (w, Ar—H, broad), 1627 (w) 1602 (C=C), 1483 (st), 1434 (st, —C—F), 1380, 1342, 1309, 1176 (Ar—S—Ar), 1142 (st), 1097, 984, 916 (st, Ar—F, bending), 828.; UV–vis (DMSO), λ_{max} (nm): 678 (Q), 647 (agg), 613, 351 (B); MS (MALDI–TOF, Ditranol as matrix) *m/z* (100%): 1232.25 [M + H]$^+$.

2,9,16,23-Tetrakis-4′-(2,3,5,6-tetrafluorophenylthio)-phthalocyaninatocobalt(II)Co(Pc) **5**

A mixture of compound **1** (0.10 g; 0.32 mmol), anhydrous $CoCl_2$ (0.01 g; 0.08 mmol; left one night in oven at 110°C), and DBU (0.05 mL) in dry quinoline was heated to 180°C under N_2 atmosphere for 8 h (1.00 mL). A similar preparation method to that used for compound **3** was used to obtain blue powder of **5**. Compound **5** is moderately soluble in $CHCl_3$ and DCM, and soluble in acetone, THF, DMF, DMSO, and quinoline.

Yield: 0.23 g (37%); mp >200°C; Anal. Calcd for $C_{56}H_{16}F_{16}N_8S_4Co$ (1291 g/mol): C, 52.05; H, 1.24; N, 8.68. Found: C, 51.93; H, 1.25; N, 8.34%. FTIR (KBr) ν (cm^{-1}): 3056 cm^{-1} (w, Ar—H, broad), 1722 (w), 1627 (w), 1606 (C=C), 1490 (st), 1434, 1380, 1313, 1234 (st, —C—F), (Ar—S—Ar), 1141, 1101, 929 (st), 893, 748, 711.; UV–vis (THF), λ_{max} (nm): 672 (Q), 632 (agg), 608, 335 (B); MS (MALDI–TOF, Ditranol as matrix) *m/z* (100%): 1295.28 $[M + H]^+$.

REFERENCES

[1] Leznoff, C. C.; Lever, A. B. P. In Phthalocyanines: Properties and Applications, Vol. 1–4; Leznoff, C. C.; Lever, A. B. P. (Eds.); VCH: Weinheim, W. Germany, 1989–1996.

[2] Gouterman, M. In The Porphyrins; Dolphin, D. (Ed.); Academic Press: New York, 1978; Vol. 3, pp. 1–65.

[3] Tau, P; Nyokong, T. Polyhedron 2006, 25, 1802.

[4] Jiang, J.; Kasuga, K.; Arnold, D. P. In Supramolecular Photosensitive and Electroactive Materials; Nalwa, H. S.; (Ed.); Academic Press: San Diego, CA, 2001; pp. 188–189 and references therein.

[5] Sadaoka, Y.; Jones, T. A.; Göpel, W. Sensors Actuators 1990, 1(1–6), 148.

[6] Simon, J. J.; Andre, H. J. In Molecular Semiconductors; Springer-Verlag: Berlin, 1985.

[7] Hanack, M.; Lang, M. Adv Mater 1994, 6, 819.

[8] Abdurrahmanoğlu, Ş.; Özkaya, A. R.; Bulut, M.; Bekaroğlu, Ö. Dalton Trans 2004, 4022.

[9] Lange, S. J.; Sibert, J. W.; Barrett, A. G. M.; Hoffman, B. M. Tetrahedron 2000, 56, 7371.

[10] De la Torre, G.; Vazquez, P.; Agullo-Lopez, F.; Torres, T. J. Mater Chem 1998, 8, 1671.

[11] Kobayashi, N.; Sasaki, N.; Higashi, Y.; Osa, T. Inorg Chem 1995, 34, 1636.

[12] Zhong, C.; Zhao, M.; Stern, C.; Barrett, A. G. M.; Hoffman, B. M. Inorg Chem 2005, 44, 8272.

[13] (a) Kandaz, M.; Yılmaz, I.; Bekaroğlu, Ö. Polyhedron 2000, 19, 115; (b) Kandaz, M.; Bekaroğlu, Ö. J Porphyrines Phthalocyanines 1999, 3, 339.

[14] Zhao, Z.; Ozoemena, K. I.; Maree, D. M.; Nyokong, T. J Chem Soc, Dalton Trans 2005, 1241.

[15] Kandaz, M.; Yaraşır, M. M. U.; Koca, A.; Bekaroğlu, Ö. Polyhedron 2002, 21, 255.

[16] Hu, Y. Y.; Laig, Q.; Shen, Y. J.; Li, Y. F. Monatsh Chem 2004, 135, 1167.

[17] Bench, B. A.; Brennessel, W. W.; Lie, H-J.; Gorun, S. M. Angew Chem, Int Ed 2002, 41, 750.

[18] (a) Noma, N.; Tsuzuki, T.; Shirota, Y. Adv Mater 1995, 7, 647; (b) Meyer, J. P.; Schlettwein, D.; Wöhrle, D.; Jaeger, N. Thin Solid Films 1995, 258, 317.

[19] Yakuphanoglu, F.; Kandaz, M.; Yarasir, M. N.; Senkal, F. B. J Phys B: Condens Matter 2007, 39, 3235.

[20] Winter, G.; Heckmann, H.; Haisch, P.; Eberhardt, W.; Hanack, M.; Luer, L.; Egelhaaf, H. J.; Oelkrug, H. J Am Chem Soc 1998, 120, 11663.

[21] Cook, M. J. J Mater Chem 1996, 6, 677.

[22] Kandaz, M.; Michel, S. L. J.; Hoffman, B. M. J Porphyrins Phthalocyanines 2003, 7, 700.

[23] Allen, M.; Sharman, W. M.; Van Lier, J. E. J Porphyrins Phthalocyanines 2001, 5, 161.

[24] Kandaz, M.; Bekaroğlu, Ö. Chem Ber 1997, 135, 1833.

[25] Kobayashi, N.; Sasaki, N.; Higashi, Y.; Osa, T. Inorg Chem 1995, 34, 1636.

[26] (a) Yarasir, M. N.; Kandaz, M.; Koca, A.; Salih, B. Polyhedron 2007, 26, 1139; (b) Kandaz, M.; Ozkaya, A. R.; Koca, A.; Salih, B. Dyes Pigments 2007, 74, 483; (c) Kalkan, A.; Guner, S.; Bayır, Z. A. Dyes Pigments 2007, 74, 636.

[27] Ozer, M.; Altindal, A.; Özkaya, A. R.; Bulut, M.; Bekaroglu, Ö. Polyhedron 2006, 25, 3593.

[28] Goldberg, D. P.; Michel, S. L. J.; White, A. J. P.; Williams, D. J.; Barrett, A. G. M.; Hoffman, B. M. Inorg Chem 1998, 37, 2100.

[29] Lever, A. B. P.; Milaeva, E. R.; Speier, G. In Phthalocyanines: Properties and Applications; Leznoff, C. C.; Lever, A. B. P. (Eds.); VCH Publishers: Weinheim, W. Germany, 1993; Vol. 3, pp. 1–69.

[30] Özkaya, A. R.; Hamuryudan, E.; Bayır, Z. A.; Bekaroğlu, Ö. J Porphyrins Phthalocyanines 2000, 4, 689.

[31] Özkaya, A. R.; Okur, A. İ.; Gül, A.; Bekaroğlu, Ö. J Coord Chem 1994, 33, 311.

[32] Özkaya, A. R.; Gürek, A.; Gül, A.; Bekaroğlu, Ö. Polyhedron 1997, 16, 1877.

[33] Özer, M.; Altındal, A.; Özkaya, A. R.; Bulut, M.; Bekaroğlu, Ö. Synth Met 2005, 155, 222.

[34] Kandaz, M.; Özkaya, A. R.; Bekaroğlu, Ö. Monatsh Chem 2001, 132, 1013.

[35] Koca, A.; Dinçer, H. A.; Koçak, M. B.; Gül, A. Russ J Electrochem 2006, 42, 31.

[36] Obirai, J.; Rodrigues, N. P.; Bedioui, F.; Nyokong, T.; J Porphyrins Phthalocyanines 2003, 7, 508.

[37] Stillman, M. J.; Nyokong, T. In Phthalocyanines: Properties and Applications; Leznoff, C. C.; Lever, A. B. P. (Eds.); VCH Publishers: Weinheim, 1993; Vol. 1, Ch. 3.

[38] (a) Balkus, K. J.; Gabriclov, G. A.; Bell, S. I.; Bedioui, F.; Roue, L.; Deevynck, J. Inorg Chem 1994, 33, 67; (b) Obirai, J.; Nyokong, T. Electrochim Acta 2005, 50, 3296; (c) Osmanbaş, Ö. A.; Koca, A.; Özçeşmeci, I.; Okur, A. I.; Gül, A. Electrochim Acta 2008, 53, 4969.